Efficient Tm:LiYF4 Lasers at $\sim$2.3 μ m: Effect of Energy-Transfer Upconversion

Pavel Loiko, Remi Soulard, Lauren Guillemot, Gurvan Brasse, Jean-Louis Doualan, Alain Braud, Aleksey Tyazhev, Ammar Hideur, Frédéric Druon, Patrice Camy

Efficient Tm:$LiYF_4$ Lasers at ~2.3 μm: Effect of Energy-Transfer Upconversion

Pavel Loiko, Rémi Soulard, Lauren Guillemot, Gurvan Brasse, Jean-Louis Doulan, Alain Braud, Aleksey Tyazhev, Ammar Hideur, Blandine Guichardaz, Frédéric Druon and Patrice Camy

***Abstract*—The $^3H_4 \rightarrow {}^3H_5$ transition of Thulium ions (Tm^{3+}), which features laser emission at ~2.3 μm is studied in details. We revise the conditions for efficient laser operation using a rate-equation model accounting for the ground-state bleaching, cross-relaxation and energy-transfer upconversion (ETU). We show that ETU has a crucial role in reaching more than unity pump quantum efficiency (QY) for ~2.3 μm Tm lasers based on highly-doped crystals. A Ti:Sapphire pumped quasi-continuous-wave 3.5 at.% Tm:$LiYF_4$ laser generated 0.73 W at 2306 nm with a record-high slope efficiency of 47.3% (versus the absorbed pump power) featuring a QY of 1.27. Diode-pumping of this crystal yielded a peak output power of >2 W. The first 2.3 μm Tm waveguide laser is also reported based on Tm:$LiYF_4$ epitaxial layers with even higher doping of 6.2 at.% generating 0.23 W with a slope efficiency of 19.8%. The spectroscopic properties of Tm:$LiYF_4$ relevant for the ~2.3 μm laser operation are revised as well.**

***Index Terms*—Solid-state lasers, laser transitions, mid-infrared, spectroscopy.**

I. Introduction

NOWADAYS, there is a great demand of mid-infrared (MIR) laser sources emitting at wavelengths around ~2.3 μm. In this spectral range, the absorption lines of such atmospheric pollutants as hydrogen fluoride (HF), carbon monoxide (CO), methane (CH_4) and formaldehyde (H_2CO) are located [1-5]. Such MIR emission falls into the 2.0–2.4 μm atmospheric window, the so-called K band. Thus, wavelength-tunable ~2.3 μm lasers are used for gas sensing in the atmosphere [1,3,5] or during the combustion experiments [2]. They are also relevant for non-invasive glucose measurements [6].

There exist several possibilities to achieve laser emission at ~2.3 μm. The first option is to use transition-metal-ion doped II-VI materials, i.e., Cr^{2+}:ZnS or Cr^{2+}:ZnSe [7,8]. However, the synthesis of zinc chalcogenide crystals and ceramics with high optical quality is complicated and, moreover, these gain media cannot be directly pumped by laser diodes. The second option is the use of semiconductor materials (GaInAs on InP or GaInAsSb on GaSb) [9-12], in Vertical-Cavity Surface-Emitting Lasers (VCSELs) with a sophisticated design.

An easier way to generate the ~2.3 μm laser emission is to use optically-pumped dielectric materials (crystals or glasses) doped with trivalent Thulium ions (Tm^{3+}). Tm^{3+} possesses an electronic configuration of $[Xe]4f^{12}$ and it is well-known for its near-infrared (NIR) laser emission at ~2 μm due to the $^3F_4 \rightarrow {}^3H_6$ transition [13], see Fig. 1(a). Tm^{3+}-doped materials are typically pumped at ~0.8 μm (to the $^3H_4$ level), e.g., using Ti:Sapphire lasers or high-power AlGaAs laser diodes. There exist a very efficient cross-relaxation (CR) process for adjacent Tm^{3+} ions which promotes this pumping scheme, $Tm_1(^3H_4) + Tm_2(^3H_6) \rightarrow Tm_1(^3F_4) + Tm_2(^3F_4)$. Thus, the pump quantum efficiency may approach 2 leading to reduced heat loading and high laser slope efficiency well exceeding the Stokes limit [14].

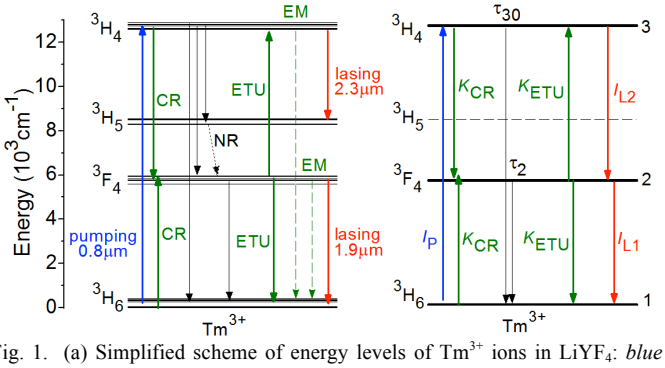

Fig. 1. (a) Simplified scheme of energy levels of Tm^{3+} ions in $LiYF_4$: *blue* and *red arrows* – pump and laser transitions, respectively, *black arrows* – radiative relaxation, green arrows - non-radiative relaxation (NR), cross-relaxation (CR), energy-transfer upconversion (ETU), energy migration (EM); (b) equivalent scheme of energy levels for construction of rate equations. The Stark splitting for Tm^{3+} ions is according to [15].

The ~2.3 μm MIR emission is related to less common Tm^{3+} transition, $^3H_4 \rightarrow {}^3H_5$ [16], Fig. 1(a). Due to the small energy gap of about 2000 cm^{-1} between the lower laser level ($^3H_5$) and

Manuscript received February 1, 2019. This work was supported by French Agence Nationale de la Recherche (ANR) through the LabEx EMC3 project FAST-MIR; European Community funds FEDER and the Normandy region. *(Corresponding author: Patrice Camy.)*

R. Soulard, P. Loiko, L. Guillemot, G. Brasse, J.-L. Doulan, A. Braud and P. Camy are with the Centre de recherche sur les Ions, les Matériaux et la Photonique (CIMAP), UMR 6252 CEA-CNRS-ENSICAEN, Université de Caen, 6 Boulevard du Maréchal Juin, 14050 Caen Cedex 4, France (e-mail: remi.soulard@oca.eu; pavel.loiko@ensicaen.fr; lauren.guillemot@ensicaen.fr; gurvan.brasse@ensicaen.fr; jean-louis.doulan@ensicaen.fr; alain.braud@ensicaen.fr; patrice.camy@ensicaen.fr).

A. Tyazhev and A. Hideur are with CORIA UMR6614, CNRS-INSA-Université de Rouen, Normandie Université, Avenue de l'université, BP. 12, 76801 Saint Etienne du Rouvray, France (e-mail: tyazheva@coria.fr; ammar.hideur@gmail.com).

B. Guichardaz is with the FEMTO-ST Institute, Route de Gray, 25030 Besançon Cedex, France (e-mail: blandine.guichardaz@femto-st.fr).

F. Druon is with the Laboratoire Charles Fabry, 2 avenue Augustin Fresnel 91127 Palaiseau, France (e-mail: frederic.druon@institutoptique.fr).

the lower-lying excited-state ($^3F_4$), the former one is rapidly depopulated by the multi-phonon non-radiative (NR) relaxation, so that the ions are accumulated in the $^3F_4$ metastable multiplet [17]. Thus, the ~2.3 μm laser transition representing a quasi-four-level laser scheme is not self-terminating.

A summary of bulk ~2.3 μm free-running and continuous-wave (CW) Tm lasers reported to date is shown in Table I. In early papers [16,18], pulsed laser operation has been achieved in Tm,Cr:$Y_3Al_5O_{12}$ and Tm,Cr:$YAlO_3$ oxide crystals (the Cr^{3+} codoping enhanced the pump absorption efficiency) under flashlamp-pumping.

Further studies were performed with laser-pumping (using Alexandrite [19] and Ti:Sapphire [17,20] lasers) allowing for selective excitation to the $^3H_4$ state. As gain materials, Tm^{3+}-doped fluoride $LiYF_4$ and oxide $Y_3Al_5O_{12}$ or $Lu_3Al_5O_{12}$ crystals were employed. A Ti:Sapphire pumped Tm:$LiYF_4$ laser generated 0.22 W at 2.30 μm with a slope efficiency of 15 % (versus the incident pump power, with 80% absorption) and a continuous tuning of the emission wavelength from 2.20 to 2.46 μm was also demonstrated [18]. Slightly higher slope efficiency was reported [20] (Table I) whilst still being lower than the Stokes efficiency for the $^3H_4 \rightarrow {}^3H_5$ laser transition (~34%).

The suitability of Yb^{3+},Tm^{3+}-codoped fluoride crystals for laser emission at ~2.3 μm was analyzed theoretically in [21].

Regarding diode-pumping which may potentially allow for power scaling, the key results were achieved for Yb^{3+},Tm^{3+}-codoped $LiYF_4$ crystals [22-24]. Here, the Yb^{3+} ions were introduced to enhance the absorption efficiency when using InGaAs laser diodes emitting at ~0.98 μm. A diode-pumped Yb,Tm:$LiYF_4$ laser generated 0.45 W at 2.30-2.32 μm (broadband emission) with a slope efficiency of 18% (with 65% pump absorption) [22].

TABLE I
SUMMARY* OF ~2.3 μM LASERS REPORTED SO FAR

Crystal	Pump**	λ_P, μm	P_{out}, W	E_{out}, mJ	λ_L, μm	η, %	Ref.
Tm,Cr:$Y_3Al_5O_{12}$	FL	–	–	–	2.32	–	[16]
	FL	–	–	150	2.32	0.4	[18]
Tm,Cr:$YAlO_3$	FL	–	–	12	2.27, 2.35	–	[16]
Tm:$LiYF_4$	AL	0.79	–	1.1	2.29–2.31	18	[19]
	TS	0.78	0.22	–	2.30	15	[17]
	TS	0.78	0.15	–	2.31	19	[20]
Tm:$Y_3Al_5O_{12}$	AL	0.79	–	1.1	2.30–2.34	14	[19]
Tm:$Lu_3Al_5O_{12}$	AL	0.79		1.0	~2.3	13	[19]
Yb,Tm:$LiYF_4$	LD	0.98	0.45	–	2.30–2.32	18	[22]
	LD	0.69+0.96	0.62	–	~2.3	7.9	[23]
Tm,Ho:$LiYF_4$	LD	0.79	0.002	–	2.08+2.31	42***	[24]
Tm:$LiYF_4$	LD	0.79	0.01	–	~2.3	10	[25]

*λ_P – pump wavelength, P_{out} and E_{out} – output power and pulse energy, respectively, λ_L – laser wavelength, η – slope efficiency. **Pumping: FL – flashlamp; AL – Alexandrite laser; TS – Ti:Sapphire laser, LD – laser diode. ***For both Tm^{3+} and Ho^{3+} emissions.

Pulsed laser operation in the passively Q-switched (PQS) [20] and mode-locked (ML) [26,27] regimes has been also achieved for ~2.3 μm bulk Tm lasers. The first ML ~2.3 μm bulk Tm laser using SEmiconductor Saturable Absorber Mirror (SESAM) generated 94 ps pulses at 2305.9 nm [27]. Shorter ML pulses of 514 fs (emission bandwidth of >15 nm) were achieved based on Kerr-lens mode-locking [26].

There also exist reports about ~2.3 μm Tm fiber lasers [28-32].

For the Tm^{3+} ions, the lifetime of the $^3H_4$ state (upper laser level for the ~2.3 μm transition) is subjected to quenching by different processes. Among them, multi-phonon NR relaxation which is strongly host-dependent, CR which raises fast with Tm^{3+} doping and energy-migration (EM) which is relevant for certain materials and high Tm^{3+} doping levels, Fig. 1(a). Thus, from the *host-material*-wise point of view, low-phonon hosts are preferred for ~2.3 μm lasers such as fluorides.

Among fluoride crystals, tetragonal lithium yttrium fluoride ($LiYF_4$) has been considered for ~2.3 μm lasers [17,19,20]. This crystal is well-known for Tm^{3+} doping and it provides highly efficient laser operation at the $^3F_4 \rightarrow {}^3H_6$ transition [33,34]. $LiYF_4$ features low maximum phonon energy, $h\nu_{ph}$ = 446 cm^{-1} [35] diminishing the NR relaxation, good thermo-mechanical properties (the thermal conductivity is about 5–7 $Wm^{-1}K^{-1}$) [36] opening the ways for power scaling, low refractive index, broad transparency range and large range of available Tm^{3+} concentrations [34]. The growth of $LiYF_4$ crystals by Czochralski method is well-developed [37]. When doped with Tm^{3+} ions, the $LiYF_4$ crystals provide long (in the ms-range) lifetimes of the excited-states ($^3H_4$ and $^3F_4$) and anisotropic emission properties [38] leading to polarized laser output.

Now, let us consider the effect Tm^{3+} *doping level* on the ~2.3 μm laser performance. At a glance, it should be kept low so that the shortening of the upper laser level ($^3H_4$) lifetime by CR is weak. In the opposite case, the laser threshold will raise significantly. However, the doping cannot be too low to keep a reasonable pump absorption efficiency. As a result of such considerations, ~2.3 μm Tm:$LiYF_4$ lasers reported to date were based on crystals with low doping levels, about 1–2 at.% [17,19,20,25].

In the present paper, we aimed to investigate the effect of two relevant energy-transfer processes, namely, the CR and energy-transfer upconversion (ETU), $Tm_1(^3F_4) + Tm_2(^3F_4) \rightarrow Tm_1(^3H_6) + Tm_2(^3H_4)$ [39], on the performance of ~2.3 μm Tm:$LiYF_4$ lasers. As a result, we prove that the ETU can play a positive role in highly Tm^{3+}-doped crystals leading to the laser slope efficiencies exceeding the Stokes limit (or, in other words, to pump quantum efficiency of more than unity).

II. SPECTROSCOPY OF TM:$LiYF_4$

A. Crystal growth

Bulk Tm:$LiYF_4$ crystals used for spectroscopic studies were grown by the Czochralski (Cz) method using undoped [001]-oriented $LiYF_4$ seeds. The growth temperature was ~780 °C. The Tm^{3+} doping concentration was 0.5, 1, 3, 5 and 10 at.%. Tetragonal $LiYF_4$ crystal (space group $C^6_{4h} - I4_1a$) is optically uniaxial (negative) and its optical axis is parallel to the crystallographic ***c***-axis. The samples were thus oriented with respect to the ***a*** and ***c*** axes.

B. $^3H_4 \rightarrow {}^3H_5$ Tm^{3+} transition

The stimulated-emission (SE) cross-sections, σ_{SE}, for the $^3H_4 \rightarrow {}^3H_5$ transition of Tm^{3+} ions in $LiYF_4$ were calculated using the Füchtbauer–Ladenburg (F-L) formula [40]:

$$\sigma_{SE}^{j}(\lambda)=\frac{\lambda^5}{8\pi n_j^2 \tau_{3rad} c}\frac{3W_j(\lambda)\beta(JJ')}{\sum_{j=\sigma,\pi,\alpha}\int \lambda W_j(\lambda)d\lambda}. \quad (1)$$

Here, $W(\lambda)$ is the measured luminescence spectrum, n is the refractive index (n_o = 1.440 and n_e = 1.462) [41], c is the speed of light, τ_{3rad} is the radiative lifetime of the emitting state ($^3H_4$), β(JJ') is the luminescence branching ratio. The index j indicates the light polarization. The transition $^3H_4 \rightarrow {}^3H_5$ is of both electric dipole (ED) and magnetic dipole (MD, ΔJ = 0, ±1) nature. Thus, for a uniaxial crystal, three principal light polarizations can be defined, i.e., σ (***E*** ⊥ ***c***, ***k*** ⊥ ***c***), π (***E*** ∥ ***c***, ***k*** ⊥ ***c***) and α (***E*** ⊥ ***c***, ***k*** ∥ ***c***) [42]. Here, ***E*** and ***k*** are the light polarization and propagation direction, respectively. Note that for purely ED transitions, π ≡ α. This difference originates from the dependence of MD transition probability on the orientation of ***H*** vector. A 1 at.% Tm:$LiYF_4$ crystal was used to measure $W(\lambda)$. The results on σ_{SE} are shown in Fig. 2(a). The maximum σ_{SE} = 0.57×10^{-20} cm^2 at 2305 nm for π-polarization. The bandwidth (FWHM) for the corresponding emission peak is 25.8 nm.

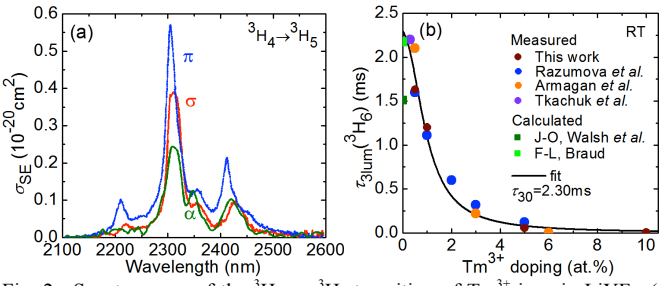

Fig. 2. Spectroscopy of the $^3H_4 \rightarrow {}^3H_5$ transition of Tm^{3+} ions in $LiYF_4$: (a) stimulated-emission (SE) cross-sections for the π, σ and α light polarizations; (b) luminescence lifetime of the $^3H_4$ state τ_{3lum} vs. the Tm^{3+} doping concentration: *symbols* – experimental data, *curve* – their fit with Eqs. (2)-(3), τ_{30} is the intrinsic lifetime. All results correspond to room temperature.

For the $^3H_4 \rightarrow {}^3H_5$ transition, the upper laser level is $^3H_4$. The results on the $^3H_4$ luminescence lifetimes τ_{3lum} obtained in the present work and in the previous papers [38,43-46] are summarized in Fig. 2(b). The τ_{3lum} decreases with the Tm^{3+} doping due to the CR effect. For the limit of very small doping concentration and, consequently, zero CR, the so-called intrinsic lifetime τ_{30} can be deduced, see Fig. 1(b) [43]:

$$1/\tau_{3lum} = 1/\tau_{30} + W_{CR}. \quad (2)$$

Here, W_{CR} is the CR rate (in s^{-1}). In Eq. (2), we do not account for other mechanisms of quenching of the $^3H_4$ lifetime such as EM which is relevant for very high Tm^{3+} doping levels above 10 at.% [47]. One should distinguish τ_{30} and the radiative lifetime τ_{3rad}. The latter is in general longer, $\tau_{3rad} \geq \tau_{30}$, because it is an inverse of the probability of solely spontaneous radiative transitions from the excited-state while τ_{30} also includes the NR relaxation rate: $1/\tau_{30} = 1/\tau_{3rad} + W_{NR}$. For $LiYF_4$ featuring a relatively low maximum phonon frequency $h\nu_{ph}$, W_{NR} is almost zero for the $^3H_4$ state [48]. Thus, $\tau_{30} \approx \tau_{3rad}$. Note that this condition is typically not satisfied in oxide materials.

The CR rate is a function of Tm^{3+} concentration [49]:

$$W_{CR} = K_{CR} N_{Tm} = C_{CR} N_{Tm}^2, \quad (3)$$

where, K_{CR} and C_{CR} are the CR macro-parameter and the CR concentration-independent micro-parameter, respectively. By using Eqs. (2)-(3), we fitted the experimental data on τ_{lum}($^3H_4$) yielding τ_{30} = 2.3±0.1 ms, Fig. 2(b). A classical way to calculate τ_{3rad} (and, thus, τ_{30}) theoretically is to use the Judd-Ofelt (J-O) theory. From the standard J-O calculations, Walsh *et al*. determined τ_{3rad}($^3H_4$) = 1.51 ms [38]. This value seems to be underestimated because longer luminescence lifetimes were measured for low doped Tm:$LiYF_4$ crystals [43,44]. Indeed, a simultaneous use of the reciprocity method (RM) and the F-L formula for transitions from the $^3H_4$ state yielded τ_{3rad} = 2.2 ms [46]. This value is in agreement with Fig. 2(b).

C. Cross-relaxation and quantum efficiency

CR is an important process defining populations of the Tm^{3+} multiplets and, thus, the laser efficiency [14]. The CR rate was determined using Eqs. (2)-(3) based on the experimental luminescence lifetimes of the $^3H_4$ state, Fig. 3(a). This figure is plotted in a double-log scale to illustrate the quadratic dependence of W_{CR} on N_{Tm}, Eq. (3). The best-fit C_{CR} = 0.25±0.03×10^{-37} s^{-1}cm^3.

There exist another way to express the CR rate constant [50]:

$$W_{CR} = \frac{1}{\tau_{30}}\left(\frac{C_{Tm}}{C_0}\right)^2, \quad (4)$$

where, C_{Tm} is the doping level (in at.%) and C_0 is the critical doping level which corresponds to a 2-fold decrease of the luminescence lifetime of the pump level ($^3H_4$). For Tm:$LiYF_4$, we calculated C_0 as 0.96 at.% (as 1 at.% Tm corresponds to the ion density of 1.38×10^{20} at/cm^3, crystal density: ρ = 3.95 g/cm^3).

The pump quantum efficiency for the $^3F_4$ state of Tm^{3+}-doped materials, η_{q1}, can exceed unity and approach 2 due to the CR effect (pumping at the $^3H_6 \rightarrow {}^3H_4$ transition) [14,49]. Assuming no ground-state bleaching and no other processes such as ETU and EM, Honea *et al*. determined η_{q1} (a ratio of ions excited to the $^3F_4$ state to the number of absorbed pump photons) as [50]:

$$\eta_{q1} = \frac{1/\tau_{30} + 2W_{CR} - (1/\tau_{3rad})(1-\beta_{32})}{1/\tau_{30} + W_{CR}}. \quad (5)$$

Here, β_{32} is the total luminescence branching ratio for the $^3H_4 \rightarrow {}^3F_4 + {}^3H_5$ transitions (due to the strong NR relaxation from

the $^3H_5$ state, both these transitions end up with the ions being at the $^3F_4$ state). As explained above, for Tm:LiYF$_4$, $\tau_{30} \approx \tau_{3rad}$. The results on η_{q1} are shown in Fig. 3(b). For very small Tm^{3+} doping, η_{q1} is limited by the β_{32} value. For more than 6 at.% Tm^{3+} doping, the theoretical pump quantum efficiency exceeding 1.95 (strong CR) is expected. The calculated results agree well with the estimation of So *et al*. based on analysis of the laser performance [39].

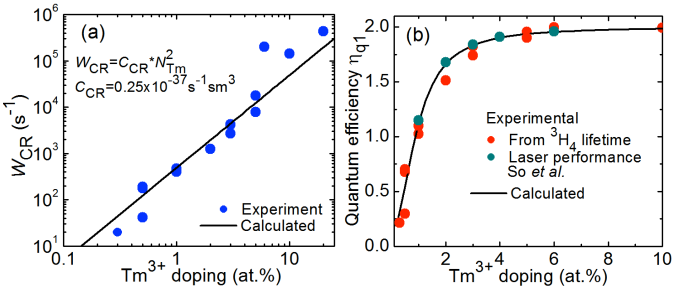

Fig. 3. Quantification of cross-relaxation in Tm:LiYF$_4$: (a) cross-relaxation rate W_{CR}: *symbols* – determined from the experimental data on $\tau_{3lum}(^3H_4)$, *line* – theoretical calculation using Eq. (3); pump quantum efficiency for the $^3F_4$ state η_{q1}: *symbols* –determined from the experimental W_{CR} rates (this work) and from the laser performance [39], *curve* – theoretical calculation using Eq. (5). All data are plotted vs. Tm^{3+} doping concentration.

In Table II, we compared the parameters defining CR (τ_{30}, C_{CR} and C_0) for several widespread Tm^{3+}-doped laser crystals [50-52]. Note that C_{CR} for Tm:LiYF$_4$ is by order of magnitude smaller that in oxide crystals because of much longer intrinsic lifetime of the $^3H_4$ state for this fluoride crystal.

TABLE II
PARAMETERS* OF CROSS-RELAXATION IN Tm^{3+}-DOPED CRYSTALS

Crystal	$\tau_{3rad}(^3F_4)$, ms	$\tau_{30}(^3F_4)$, ms	C_{CR}, 10^{-37} cm^6/s	C_0, at.%	Ref.
Tm:LiYF$_4$	~2.2 [46]	2.3	0.25	0.96	This work
Tm:Lu$_2$O$_3$	0.69	0.35	1.25	0.53	[51]
Tm:Y$_3$Al$_5$O$_{12}$	1.44	0.54	3.95	0.50	[50]
Tm:KLu(WO$_4$)$_2$	>>0.20	0.24	2.7	1.94	[52]

*τ_{3rad} and τ_{30} – radiative and intrinsic (unquenched) lifetimes of the $^3F_4$ Tm^{3+} state, respectively; C_{CR} – CR concentration-independent micro-parameter; C_0 – critical Tm^{3+} doping level.

D. Energy-transfer upconversion

Energy-transfer upconversion in Tm:LiYF$_4$, $^3F_4 + {}^3F_4 \rightarrow {}^3H_4 + {}^3H_6$, is a phonon-assisted process which is detrimental for the ~1.9 μm laser transition [39] but can be useful for the ~2.3 μm one.

To quantify ETU, we excited Tm:LiYF$_4$ crystals directly to the $^3F_4$ state (at 1.68 μm) and monitored power dependence of luminescence from the $^3H_4$ (at ~1.5 μm) and $^3F_4$ (at ~1.9 μm) multiplets. The observation of the former emission is a direct evidence of ETU. From the ratio of integrated intensities of these emissions, we deduced the ratio of the populations $N(^3H_4)/N(^3F_4)$, see Fig. 4(a). This ratio was also calculated numerically using a rate-equation model accounting for the ground-state bleaching, CR, ETU and spatial distribution of the pump, as shown by the curves in Fig. 4(a). From such a modeling, we determined the ETU parameter K_{ETU} which amounted to 3.5±1, 14.5±2 and 22±5×10^{-20} cm^{3}s^{-1} for 3, 4 and 5 at.% Tm-doping, respectively. As expected, K_{ETU} increases with the Tm^{3+} concentration.

A summary of K_{ETU} values for Tm:LiYF$_4$ reported to date is presented in Fig. 4(b). In [48,53], K_{ETU} was determined from luminescence-decay measurements. In [54], we determined it from the modeling of the laser performance and in [55], it was calculated theoretically. For Tm^{3+} doping below 6 at.% which is common for laser crystals, the results on K_{ETU} are in relative agreement with each other while for higher doping, a strong discrepancy is observed.

The concentration dependence of K_{ETU} has been previously expressed by a linear law using a concentration-independent micro-parameter C_{ETU} [49]:

$$K_{ETU} = C_{ETU} N_{Tm}. \quad (6)$$

In our case, C_{ETU} = 3.9±1×10^{-40} cm^{6}s^{-1} and it is by two orders of magnitude smaller than C_{CR}. However, the K_{ETU} parameters of Tm:LiYF$_4$ are high enough to ensure efficient 2.3 μm laser operation of this crystal, as will be shown below. Note the concentration dependence of K_{ETU} seems to be faster than linear and well fitted with a quadratic curve, Fig. 4(b).

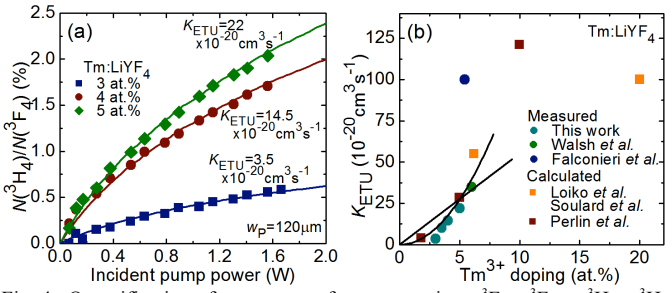

Fig. 4. Quantification of energy-transfer upconversion, $^3F_4 + {}^3F_4 \rightarrow {}^3H_4 + {}^3H_6$, in Tm:LiYF$_4$: (a) ratios of the fractional populations of the $^3H_4$ and $^3F_4$ Tm^{3+} multiplets for the 1.68 μm excitation (pump spot radius: w_P = 120 μm) *vs*. the incident pump power for various Tm^{3+} concentrations: *symbols* – experimental data, *curves* – their rate-equation modeling yielding K_{ETU} values; (b) summary of the ETU parameters reported to date, *line* and *quadratic curve* represent their possible concentration-dependences.

III. BULK LASERS AT ~2.3 μM

A. Laser set-up

The laser experiments started using bulk Tm:LiYF$_4$ crystal. The laser crystal was an ***a***-cut 3.5 at.% Tm:LiYF$_4$ having a cylindrical shape (diameter: 8.5 mm, length: 8.1 mm). The actual Tm^{3+} ion density N_{Tm} = 4.83×10^{20} cm^{-3}. Both its faces were polished to laser quality and antireflection (AR) coated for ~1.9 μm. The crystal was mounted on a Cu-holder using a silver thermal paste and it was passively cooled.

The scheme of the laser set-up is shown in Fig. 5. A hemispherical laser cavity was formed by a flat pump mirror (PM) coated for high transmission (HT) at the pump wavelength (T = 81% at 0.79 μm) and at ~1.9 μm (the $^3F_4 \rightarrow {}^3H_6$ Tm^{3+} emission) and for high reflection (HR) at ~2.3 μm, and a set of concave output couplers (OCs) with the radius of curvature of 100 mm and a transmission T_{OC} of 0.7%, 1.3% and 4.0% at 2.3 μm. Due to the R = 95% reflection from the OCs at the pump wavelength, the crystal was pumped in a

double-pass. Moreover, to suppress further the ~1.9 μm emission, all the OCs provided HT (T > 90%) at this wavelength. The geometrical cavity length was about 100 mm.

As the first pump source, we used a CW Ti:Sapphire laser (model 3900S, Spectra Physics) delivering 3.2 W at 0.79 μm ($M^2 \approx 1$). The pump power incident on the crystal was varied using a rotatory λ/2 plate and a Glan-Taylor polarizer. The pump polarization in the crystal corresponded to π. The pump beam was focused by a spherical lens (focal length: f = 150 mm) resulting in a spot radius w_P of 61 μm and a confocal parameter $2z_R$ of 4.2 cm. The pump beam was mechanically modulated using a chopper (duty cycle: 1:2, pulse duration: ~10 ms) leading to quasi-CW pumping.

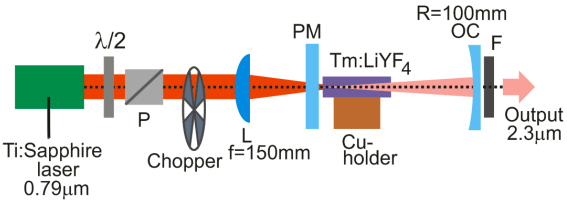

Fig. 5. Scheme of the ~2.3 μm Tm:$LiYF_4$ bulk laser pumped by a Ti:Sapphire laser: λ/2 – rotatory half-wave plate, P – Glan-Taylor polarizer, L – lens, PM – pump mirror, OC – output coupler, F – cut-off filter.

The second pump source was a fiber-coupled AlGaAs laser diode (DILAS, fiber core diameter: 105 μm, numerical aperture, N.A.: 0.22) emitting up to 28 W of unpolarized output at a wavelength of 793.2 nm (emission bandwidth: <4 nm, $M^2 \approx 46$). The pump beam was collimated and focused by a pair of spherical lenses (f = 50 mm and 150 mm, respectively) resulting in w_P of 150 μm and a Rayleigh length z_R of 5.7 mm. The pump beam was electrically modulated (duty cycle: 1:20, pulse duration: ~10 ms). Due to the strong divergence of the pump, during the second pump pass (after the reflection from the OC), the diameter of the pump beam in the crystal was ~1.5 mm thus producing minor effect on inversion in the laser crystal. Consequently, the pumping was considered in single-pass.

The radius of the laser mode w_L in the crystal was estimated within the ABCD formalism to be 70 μm (taking into account thermal lens in the crystal).

The laser emission spectra were measured using an optical spectrum analyzer (OSA, model AQ6375B, Yokogawa). The laser output was filtered from the residual pump using a cut-off filter (FEL 900, Thorlabs).

B. Results: Ti:Sapphire pumping

First, we describe the results achieved using the Ti:Sapphire pumping. For all studied OCs, the laser operated solely at the $^3H_4 \rightarrow {}^3H_5$ transition with no emission at ~1.9 μm. The laser output was linearly polarized; the polarization was determined by the gain anisotropy (π), see Fig. 2(a).

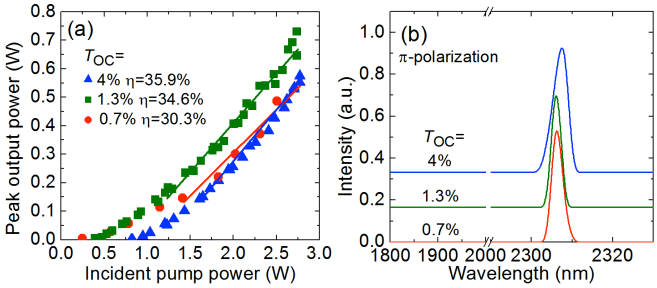

Fig. 6. Ti:Sapphire pumped ~2.3 μm Tm:$LiYF_4$ bulk laser: (a) input-output dependences, η – slope efficiency; (b) typical laser emission spectra. The laser polarization is π. The pumping is quasi-CW (duty cycle: 1:2).

The maximum peak output power was achieved using 1.3% OC, namely 0.73 W at 2306 nm with a slope efficiency η of 34.6% (*vs.* the incident pump power P_{inc}). The input-output dependence was nonlinear close to the laser threshold (at P_{inc} = 0.40 W). Because of this, the fit for the determination of η was performed for pump powers of about 3 times higher than the threshold value, Fig. 6(a). The maximum optical-to-optical efficiency η_{opt} was 26.7%. For higher T_{OC} = 4%, the laser operated with slightly higher slope efficiency (35.9%) whilst with lower peak output power of 0.55 W at 2305 nm and much higher laser threshold of 0.81 W. Further power scaling was limited by the available pump power. No thermal roll-over of the input-output dependences or crystal fracture were observed during the laser experiments.

The passive losses in the crystal were estimated to be 0.5% using the Findlay-Clay analysis [56].

The laser emission spectra for all OCs were similar, Fig. 6(b).

We have also studied true CW performance of this laser for the optimum 1.3% OC (i.e., when removing the chopper from the pump beam). The P_{inc} value was limited to approximately half of the available power, ~1.5 W. The achieved CW output power was similar to the peak power achieved under quasi-CW regime. The maximum output power reached 0.24 W.

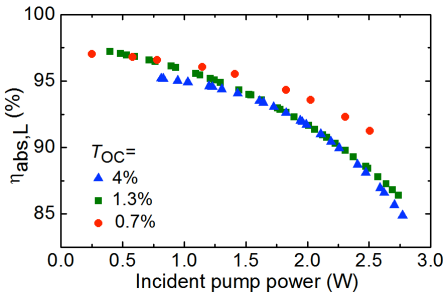

Fig. 7. Pump absorption under lasing conditions $\eta_{abs,L}$ for 3.5 at.% Tm:$LiYF_4$ crystal (Ti:Sapphire pumping, w_P = 61 μm).

The pump absorption under lasing conditions $\eta_{abs,L}$ was determined by measuring the residual pump power after the OC with a short-pass filter. The results are shown in Fig. 7. The saturation of absorption was observed. In particular for 1.3% OC, $\eta_{abs,L}$ decreased from 97.2% to 86.3% when the pump power increased from the laser threshold to its maximum value, i.e., from 0.40 to 2.74 W. For other OCs, a similar behavior was observed.

According to the measured pump absorption, the slope efficiency vs. the absorbed pump power P_{abs} for the 1.3% and 4% OCs reached 47.3% and 51.7%, respectively. Here, the fit of the input-output dependence was performed starting from the pump power well above the laser threshold as explained above. Thus, this work represents the best results in terms of output power and slope efficiency for any laser-pumped 2.3 μm laser, cf. Table I.

C. *Results: diode-pumping*

The results for diode-pumping are shown in Fig. 8. For all OCs, the laser generated a linearly polarized emission (π) at ~2306 nm. The input-output dependences were linear. For 1.3% OC, the laser generated a maximum peak output power of 2.4 W (average power: 0.12 W) with η = 11.5%. The laser threshold was at P_{inc} = 2.0 W and η_{opt} amounted to 10.3%. For higher output coupling, the laser performance deteriorated. The input-output dependences were linear up to at least P_{inc} = 23.2 W.

The pump absorption $\eta_{abs,L}$ was weakly dependent on the OC and the pump power and amounted to 60%. Thus, the maximum slope efficiency vs. the absorbed pump power was 19.2% (for T_{OC} = 1.3%) which is much lower than in the case of Ti:Sapphire pumping.

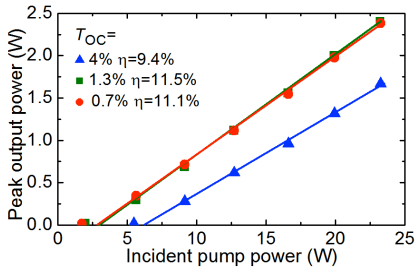

Fig. 8. Input-output dependences of diode-pumped ~2.3 μm Tm:$LiYF_4$ bulk laser, η – slope efficiency. The laser polarization is π. The pumping is quasi-CW (duty cycle: 1:20).

D. *Modeling of the laser performance*

For modeling of the laser performance, we will consider the results achieved under Ti:Sapphire pumping. The model will account for ground-state bleaching, CR and ETU. The system of rate equations for Tm^{3+} ions is as following:

$$\frac{dN_2}{dt} = 2K_{CR}N_1N_3 - 2K_{ETU}N_2^2 - \frac{N_2}{\tau_2} + \sigma_{SE}^{L2}I_{L2}N_3, \quad (7a)$$

$$\frac{dN_3}{dt} = \sigma_{abs}^{P}I_P N_1 - K_{CR}N_1N_3 + K_{ETU}N_2^2 - \frac{N_3}{\tau_{30}} - \sigma_{SE}^{L2}I_{L2}N_3, \quad (7b)$$

where, N_i (i = 1, 2, 3) is the ion density for the i-th level, Fig. 1(b), $N_1 + N_2 + N_3 = N_{Tm}$, t is time, $K_{CR} = W_{CR}/N_{Tm}^2$ is the CR macroscopic parameter expressed in cm^3s^{-1}, τ_2 is the lifetime of the 2nd level ($^3F_4$), τ_{30} is the intrinsic (unquenched) lifetime of the 3rd level ($^3H_4$), σ^{L2}_{SE} is the SE cross-section at the laser frequency ν_{L2} ($^3H_4 \rightarrow {}^3H_5$) σ^{P}_{abs} is the absorption cross-section at the pump frequency ν_P, I_P and I_{L2} are the pump and laser intensities expressed in photons/(s·cm²). We will neglect the radiative decay in the 3 → 2 channel because the corresponding luminescence branching ratio β_{32} is small [38]. In Eq. (7), we assume no lasing at the $^3F_4 \rightarrow {}^3H_6$ transition with a frequency ν_{L1} (so that $I_{L1} \equiv 0$).

In the *first* approach, we will derive the pump quantum efficiency for the $^3H_4 \rightarrow {}^3H_5$ transition η_{q2} from the measured output power of the laser P_{out}. According to the definition of η_{q2} (the ratio of the number of emitted photons at ~2.3 μm to the number of absorbed pump photons), from the formalism of the rate equations, we have:

$$\eta_{q2} = \frac{\frac{N_3}{\tau_{30}} + \sigma_{SE}^{L2}I_{L2}N_3}{\sigma_{abs}^{P}I_P N_1}. \quad (8)$$

The population of the upper laser level N_3 can be estimated from the threshold condition (gain is equal to losses):

$$\sigma_{SE}^{L2}N_3\ell = \frac{T_{OC}+L}{2}. \quad (9)$$

Here, ℓ is the thickness of the crystal and L are the passive losses. In this equation, we neglect the axial dependence of the population N_3. By deriving N_3 from Eq. (9) and substituting it into Eq. (8), we determined I_{L2} and, then, the output laser intensity $I_{out} = T_{OC}\cdot(I_{L2}/2)$. The output power P_{out} is then given by:

$$P_{out} = h\nu_{L2}\pi w_L^2 I_{out}, \quad (10a)$$

$$P_{out} = \frac{h\nu_{L2}}{h\nu_P}\frac{w_L^2}{w_P^2}\frac{T_{OC}}{T_{OC}+L}\eta_{q2}\eta_{abs}P_{inc} - \frac{T_{OC}h\nu_{L2}\pi w_L^2}{2\sigma_{SE}^{L2}\tau_{30}}. \quad (10b)$$

Here, w_L is the radius of the laser mode in the crystal and we have also taken into account that the pump absorption $\eta_{abs} = \sigma^{P}_{abs}N_1\ell$ and the incident pump power $P_{inc} = h\nu_P\pi w_P^2 I_P$. The first term of Eq. (10b) represents an expression for the laser slope efficiency *vs.* the absorbed pump power $P_{abs} = \eta_{abs}\cdot P_{inc}$ containing four factors: the Stokes efficiency $\eta_{St} = h\nu_{L2}/h\nu_P$, the mode overlap efficiency $\eta_{mode} = w_L^2/w_P^2$ (we assume $\eta_{mode} \approx 1$), the output-coupling efficiency $\eta_{OC} = T_{OC}/(T_{OC}+L)$ and the pump quantum efficiency η_{q2}. From Eq. (10b), the laser threshold is:

$$P_{th} = h\nu_P\pi w_P^2\frac{T_{OC}+L}{2\sigma_{SE}^{L2}\tau_{30}\eta_{q2}\eta_{abs}}. \quad (11)$$

Using Eq. (10b), we were able to determine η_{q2} for each point at the input-output laser dependence from Fig. 6(a).

The calculated η_{q2} values are shown in Fig. 9. For all studied OCs, the quantum efficiency gradually increases with the incident pump power. The variation is from 0.14 to 1.27 for the optimum 1.3% OC. The values of η_{q2} exceeding unity represent a direct evidence of the effect of ETU on the laser performance. Indeed, ETU is responsible for re-feeding the upper laser level ($^3H_4$) at the expense of the $^3F_4$ population. The fact that η_{q2} is well below unity close to the laser

threshold clearly represents the effect of CR which is a detrimental process decreasing the upper laser level population.

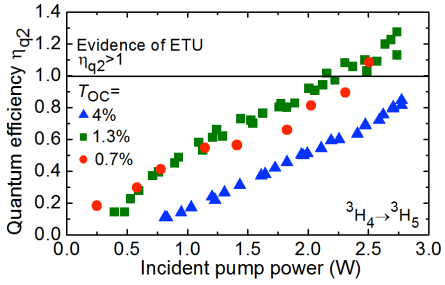

Fig. 9. Pump quantum efficiency for the $^3H_4 \rightarrow {}^3H_5$ laser channel (pumping to the $^3H_4$ state) η_{q2} calculated using Eq. (10b).

To reveal the effect of CR and ETU on the pump quantum efficiency, we have derived another expression for η_{q2} based on the populations of the Tm^{3+} multiplets. In the steady-state conditions ($dN_i/dt = 0$), by combining Eq. (8) and Eq. (7b), we obtained:

$$\eta_{q2} = 1 - \frac{K_{CR} N_1 N_3}{\sigma^P_{abs} I_P N_1} + \frac{K_{ETU} N_2^2}{\sigma^P_{abs} I_P N_1}. \quad (12)$$

This equation shows that that there exist two competitive energy-transfer processes which determine η_{q2}, namely CR and ETU. If both processes are negligible (an ideal case of almost zero doping concentration), $\eta_{q2} \equiv 1$ and the laser slope efficiency will be limited by the Stokes efficiency. If there is no ETU, the quantum efficiency will be less than unity due to CR. Finally, if there are two processes (CR and ETU), η_{q2} may exceed unity as observed in Fig. 9.

There exist upper limit for η_{q2}. By combining Eq. (12), the rate-equation, Eq. 7(a), at the steady-state ($dN_2/dt = 0$), and the intuitive expression for η_{q2}, Eq. (8), we obtain:

$$\eta_{q2} = 2 - \frac{1}{\sigma^P_{abs} I_P N_1}\left(\frac{N_3}{\tau_{30}} + \frac{N_2}{\tau_2}\right). \quad (13)$$

From this equation, $\eta_{q2} \le 2$. The upper limit can be reached for a material exhibiting strong ETU and long lifetimes of the $^3H_4$ and $^3F_4$ multiplets and pumped well above the laser threshold when the laser operates solely at the $^3H_4 \rightarrow {}^3H_5$ transition, so that the $^3H_4$ level is depopulated by ~2.3 μm laser emission and the $^3F_4$ one is depopulated by ETU.

From these considerations, it is possible to explain the decrease of pump absorption η_{abs} (bleaching) with the pump power, Fig. 7. This is because when there is no laser operation at the $^3F_4 \rightarrow {}^3H_6$ transition, the population of the ground-state $^3H_6$ is not clamped by the threshold condition. Thus, with an increased pump power, the ground-state is depopulated while the Tm^{3+} ions are accumulated in the metastable intermediate $^3F_4$ state. Note that when the laser operates at both the $^3H_4 \rightarrow {}^3H_5$ and $^3F_4 \rightarrow {}^3H_6$ transitions simultaneously, η_{abs} is expected to be nearly constant with the pump power.

Within the *second* approach, we solved the system of rate equations, Eq. (7), numerically accounting for the spatial and axial distribution of the pump and laser fields in the crystal. Then, the laser output power at ~2.3 μm was determined from Eq. (10a) and η_{q2} was determined from Eq. (12).

First, we performed the calculations assuming that the laser operates solely at the $^3H_4 \rightarrow {}^3H_5$ transition ($I_{L1} \equiv 0$). Three different Tm^{3+} doping levels of 1.5, 3.5 and 6.5 at.% were considered. The CR and ETU parameters were as following: $K_{CR} = 0.52$, 1.21 and 2.24×10^{-17} cm^3s^{-1} and $K_{ETU} = 0.3$, 1.4 and 4.5×10^{-19} cm^3s^{-1}, respectively. The calculations were done under two assumptions: (i) there exist both CR and ETU processes ($K_{CR} \neq 0$, $K_{ETU} \neq 0$); (ii) there exist only CR while ETU is absent ($K_{CR} \neq 0$, $K_{ETU} = 0$). The spectroscopic parameters of Tm^{3+} ions were as following: $\sigma^{L2}_{SE} = 0.57\times10^{-20}$ cm^2, $\sigma^P_{abs} = 0.63\times10^{-20}$ cm^2 at 791 nm (for π-polarization) [46], $\tau_{30} = 2.3$ ms, $\tau_2 = 10$ ms [46]. The incident pump power was fixed ($P_{inc} = 3.0$ W).

The results on the output power at ~2.3 μm are presented in Fig. 10(a). When there is no ETU in the system ($K_{CR} \neq 0$, $K_{ETU} = 0$), for a fixed (small) radius of the laser mode (e.g., $w_L = 60$ μm as in our case), the output power slightly increases with the Tm^{3+} doping due to the increased pump absorption. When the ETU is present ($K_{CR} \neq 0$, $K_{ETU} \neq 0$), the output power is greatly increased and this effect becomes more evident for higher Tm^{3+} doping levels because the action of ETU against CR is enhanced. Moreover, for each Tm^{3+} concentration, there is an optimum radius of the laser mode maximizing the output power. With an increase of the Tm^{3+} doping, the optimum w_L value decreases. For 3.5 at.% Tm-doping, the laser geometry used in the present work, cf. Fig. 5, provided almost optimum w_L value.

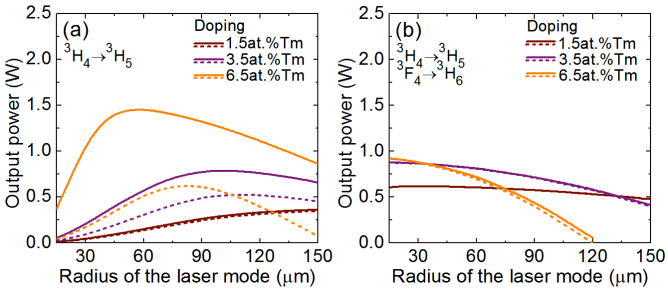

Fig. 10. Calculated output power at ~2.3 μm of a diode-pumped Tm:$LiYF_4$ laser with different doping levels, *solid curves* – $K_{CR} \neq 0$, $K_{ETU} \neq 0$, *dashed ones* - $K_{CR} \neq 0$, $K_{ETU} = 0$: (a) the laser operating at the $^3H_4 \rightarrow {}^3H_5$ transition only; (b) the laser operating at both the $^3H_4 \rightarrow {}^3H_5$ and $^3F_4 \rightarrow {}^3H_6$ transitions simultaneously. The Tm^{3+} doping is 1.5, 3.5 and 6.5 at.%, $P_{inc} = 3.0$ W, $T_{OC} = 2.0\%$, $L = 0.2\%$, $\ell = 9.0$ mm.

Furthermore, we have analyzed the laser performance for operation at both the $^3H_4 \rightarrow {}^3H_5$ and $^3F_4 \rightarrow {}^3H_6$ transitions simultaneously. For this, the term $-\sigma^{L1}_{SE} I_{L1} N_2$ representing stimulated-emission at ν_{L1} (at ~1.9 μm) was added to the rate-equation, Eq. (7a). The results are shown in Fig. 10(b). In this case, the effect of ETU on the laser performance is minor because population of the $^3F_4$ state is clamped by the threshold condition for the $^3F_4 \rightarrow {}^3H_6$ laser. For a fixed (small) w_L, the output power only slightly increases with Tm^{3+} doping due to

the increased pump absorption and finally saturates.

To conclude, the simultaneous operation of the Tm lasers at both the $^3H_4 \rightarrow {}^3H_5$ and $^3F_4 \rightarrow {}^3H_6$ transitions is mostly detrimental for their ~2.3 μm laser performance, especially at high doping levels. Moreover, in the case of single laser operation ($^3H_4 \rightarrow {}^3H_5$) the efficiency of the ~2.3 μm laser can be greatly enhanced by using highly Tm^{3+}-doped crystals due to the ETU effect.

The existence of the optimum size of the laser mode for the ~2.3 μm Tm:$LiYF_4$ laser operating solely at the $^3H_4 \rightarrow {}^3H_5$ transition is due to (i) strong dependence of pump absorption η_{abs} or, equivalently, ground-state bleaching, on the pump spot radius w_P (notice that in this modeling, we assumed $w_L \approx w_P$), see Fig. 11(a), and (ii) increase of the laser threshold with increasing pump spot size. Physically, the first effect is explained as following: if there is no laser operation at the $^3F_4 \rightarrow {}^3H_6$ transition, the population of the ground-state ($^3H_6$) is not clamped by the threshold condition and thus it can be depopulated for high pump intensities (for small w_P). ETU increases the pump absorption because it brings excited Tm^{3+} ions back to the ground-state. Thus, the optimum size of the laser mode decreases with Tm^{3+} doping due to enhanced ETU.

When the laser operates at both the $^3H_4 \rightarrow {}^3H_5$ and $^3F_4 \rightarrow {}^3H_6$ transitions simultaneously, the size of the pump mode and ETU have minor action on the pump absorption, Fig. 11(b).

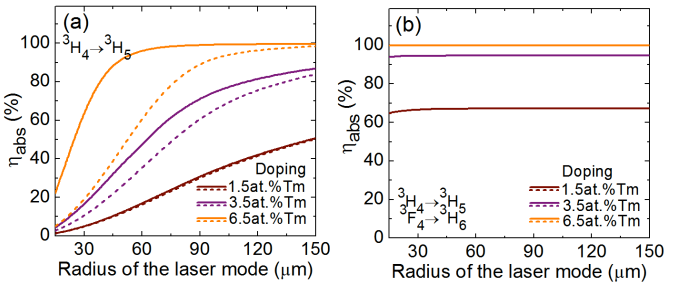

Fig. 11. Calculated pump absorption η_{abs} for a diode-pumped Tm:$LiYF_4$ laser with different doping levels, *solid curves* – $K_{CR} \neq 0$, $K_{ETU} \neq 0$, *dashed ones* - $K_{CR} \neq 0$, $K_{ETU} = 0$: (a) the laser operating at the $^3H_4 \rightarrow {}^3H_5$ transition only; (b) the laser operating at both the $^3H_4 \rightarrow {}^3H_5$ and $^3F_4 \rightarrow {}^3H_6$ transitions simultaneously. The parameters used for modeling are listed in the text.

In Fig. 12, the calculated pump quantum efficiency η_{q2} for the Tm:$LiYF_4$ laser is shown. When the laser operates solely at the $^3H_4 \rightarrow {}^3H_5$ transition and there is no ETU in the system ($K_{CR} \neq 0$, $K_{ETU} = 0$), the η_{q2} value has an upper limit of 1 and it has almost no dependence on the Tm^{3+} doping level for small radii of the pump mode. If the ETU is present ($K_{CR} \neq 0$, $K_{ETU} \neq 0$), the pump quantum efficiency greatly increases with Tm^{3+} doping approaching the upper limit of 2, Fig. 12(a). Note that for about 1–2 at.% Tm-doping which was typically used in the previous studies [17,19,20,25], η_{q2} is below 1 which agrees with the observed laser slope efficiencies. For 3.5 at.% Tm-doping, as in our case, $\eta_{q2} > 1$ can be observed, cf. Fig. 9.

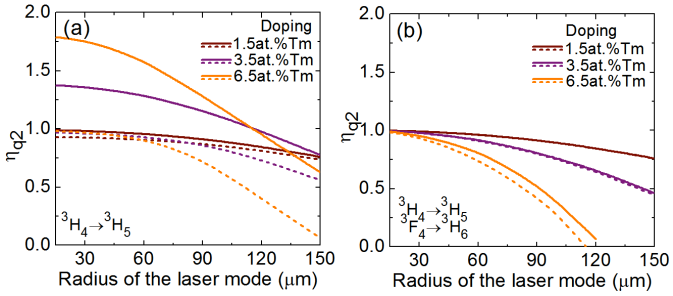

Fig. 12. Calculated pump quantum efficiency η_{q2} for for a diode-pumped Tm:$LiYF_4$ laser with different doping levels, *solid curves* – $K_{CR} \neq 0$, $K_{ETU} \neq 0$, *dashed ones* - $K_{CR} \neq 0$, $K_{ETU} = 0$: (a) the laser operating at the $^3H_4 \rightarrow {}^3H_5$ transition only; (b) the laser operating at both the $^3H_4 \rightarrow {}^3H_5$ and $^3F_4 \rightarrow {}^3H_6$ transitions simultaneously. The parameters used for modeling are listed in the text.

When the laser operates at both the $^3H_4 \rightarrow {}^3H_5$ and $^3F_4 \rightarrow {}^3H_6$ transitions simultaneously, η_{q2} cannot exceed unity even under the conditions of high Tm^{3+} doping and, consequently, strong ETU, Fig. 12(b).

Using the above described second approach, we calculated the values of the maximum output power P_{out}, threshold power P_{th}, slope efficiency η (vs. the incident pump power) and the maximum pump quantum efficiency $\eta_{q2(max)}$ for the studied 3.5 at.% Tm:$LiYF_4$ laser, see Table III. The results of calculation are in reasonable agreement with the experimental data.

This confirms the first observation of more than unity pump quantum efficiency η_{q2} for the ~2.3 μm laser transition in bulk Tm:$LiYF_4$.

TABLE III
LASER PERFORMANCE* OF ~2.3 μM BULK TM:$LIYF_4$ LASERS

T_{OC}	Data	P_{out}, W	P_{th}, W	η, %	$\eta_{q2(max)}$
0.7%	Exp.	0.49	0.24	30.3	**1.08**
	Calc.	*0.52*	*0.24*	*20.8*	***1.30***
1.3%	Exp.	0.73	0.40	34.6	**1.27**
	Calc.	*0.65*	*0.36*	*27.2*	***1.23***
4%	Exp.	0.55	0.81	35.9	**0.85**
	Calc.	*0.63*	*0.99*	*36.3*	***0.93***

*P_{out} – output power, P_{th} – threshold incident power, η – slope efficiency *vs.* the incident pump power, $\eta_{q2(max)}$ – pump quantum efficiency at the maximum pump power.

IV. WAVEGUIDE LASERS AT ~2.3 μM

A. *Fabrication of waveguides*

Single-crystalline 6.2 at.% Tm, 3.5 at.% Gd:$LiYF_4$ thin film was grown on undoped (001)-oriented $LiYF_4$ substrate by the Liquid Phase Epitaxy (LPE) method [54]. The actual Tm^{3+} ion density $N_{Tm} = 8.56\times10^{20}$ cm^{-3}. The optically passive Gd^{3+} ions were added to enhance the refractive index contrast between the active layer and the substrate ($\Delta n = 2.3\pm0.5\times10^{-3}$). The film thickness was 30 μm.

The films were further microstructured by diamond saw dicing resulting in surface channel (ridge) waveguides (WGs) oriented along the ***a***-axis and having a square cross-section of 30×30 μm^2. The length of the WGs was 8.0 mm. The WG propagation losses were 0.28±0.1 dB/cm at ~1.9 μm. More details can be found in [54].

B. *Laser set-up*

The scheme of the waveguide laser is shown in Fig. 11. The sample with the WG was mounted on a Cu-holder using a silver thermal paste. It was passively cooled. The laser cavity was composed of a flat PM coated for HR at 1.88-2.32 μm and HT at the pump wavelength (T = 69% at 0.79 μm), and a set of two flat OCs coated for HT at 1.83-1.88 μm (T = 90% / 97%) and having a transmission of 4% / 1.3% at 2.3 μm, respectively. Both PM and OC were placed as close as possible to the WG end-facets. No index-matching liquid was used to avoid damage of the optical elements.

As a pump source, we used the same Ti:Sapphire laser, see Section IIIA. The pump polarization corresponded to π in the WG. The pump beam was focused by an uncoated CaF_2 spherical lens (f = 40 mm, T = 93.8% at 0.79 μm) providing a pump spot diameter at the input face of the WG $2w_P$ of ~30 μm. The pump coupling efficiency η_{coupl} was determined from pump-transmission measurements at 0.84 μm (out of Tm^{3+} absorption) to be 87±1%. The pump absorption at the laser threshold $\eta_{abs(1\text{-}pass)}$ was measured to be 71.0±0.5%. Both OCs provided partial reflection at the pump wavelength (R = 93% / 96%, respectively) and thus the WG was pumped in a double-pass. The calculated total pump absorption $\eta_{abs(2\text{-}pass)}$ amounted to 90.1%. The pump beam was mechanically modulated using a mechanical chopper (1:2 duty cycle, 10 ms pump pulses).

The WG laser operated at the fundamental transverse mode. The mode radius w_L was 15 μm.

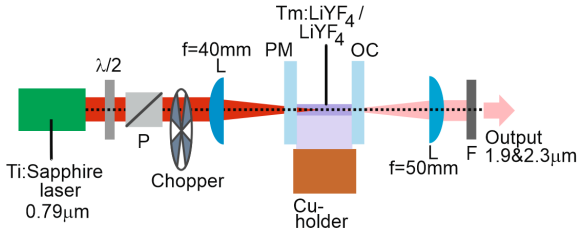

Fig. 13. Scheme of the ~2.3 μm Tm:$LiYF_4$ channel WG laser: λ/2 – rotatory half-wave plate, P – Glan-Taylor polarizer, L – lens, PM – pump mirror, OC – output coupler, F –cut-off / bandpass filter.

The output laser beam was collimated using a spherical lens (f = 50 mm). The total output power was determined after filtering the residual pump using a cut-off filter (FEL 900, Thorlabs). The power at ~2.3 μm was separately determined using a bandpass filter (FB2250-500, Thorlabs).

C. *Laser performance*

The WG Tm:$LiYF_4$ laser operated at both ~1.9 μm and ~2.3 μm transitions for both OCs. The laser output was linearly polarized (π).

The best results were achieved using the output coupler having a transmission of 90% / 4% at ~1.9 μm / 2.3 μm. The maximum peak total output power reached 1.13 W with a total slope efficiency η^{Σ} of 64.2% (*vs.* the coupled pump power). The laser threshold was at 0.10 W and the total optical-to-optical efficiency η^{Σ}_{opt} amounted to 59.4%. Near the threshold, the laser operated solely at the $^3F_4 \rightarrow {}^3H_6$ transition. For the pump power exceeding 0.68 W, the emission due to the $^3H_4 \rightarrow {}^3H_5$ transition appeared, as shown in Fig. 11(a). The corresponding peak output power reached 0.23 W with η = 17.8%. According to the pump absorption efficiency $\eta_{abs(2\text{-}pass)}$, the slope efficiency vs. the absorbed pump power was 19.8% being smaller than in the bulk laser. For the second studied OC, the laser performance was inferior.

The typical spectra of the laser emission are shown in Fig. 11(b). The emission corresponding to the $^3F_4 \rightarrow {}^3H_6$ transition occurred at 1877-1881 nm in agreement with the gain spectra for π-polarization. The $^3H_4 \rightarrow {}^3H_5$ laser transition operated at 2304-2307 nm (both for T_{OC} = 90% / 4%). The multi-peak spectral behavior for both transitions is due to the etalon effects at the WG / mirror interfaces.

The achieved results represent the first ~2.3 μm thulium *waveguide* laser.

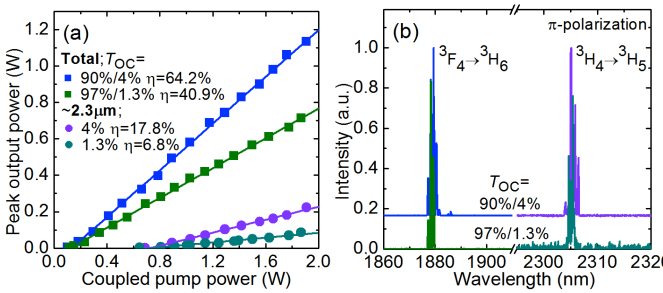

Fig. 14. Ti:Sapphire pumped ~1.9 μm & 2.3 μm Tm:$LiYF_4$ waveguide laser: (a) input-output dependences, η – slope efficiency; (b) typical laser emission spectra. The laser polarization is π. The pumping is quasi-CW (duty cycle: 1:2).

D. *Modeling of laser performance*

The performance of the WG laser was modeled numerically using the second approach described above. The results of this modeling are summarized in Table IV. Here, P^{Σ}_{out} is the total output power (for both the $^3H_4 \rightarrow {}^3H_5$ and $^3F_4 \rightarrow {}^3H_6$ laser transitions), P^{Σ}_{th} is the corresponding laser threshold and η^{Σ} is the corresponding slope efficiency (both *vs.* the coupled pump power). The values without the "Σ" superscript refer solely to the ~2.3 μm emission. For the WG laser, it was not possible to derive the η_{q2} value from the output power (using the first approach) because of simultaneous operation of the laser at ~1.9 μm and ~2.3 μm.

TABLE IV
LASER PERFORMANCE* OF ~2.3 μM WAVEGUIDE TM:$LiYF_4$ LASERS

T_{OC}	Data	P^{Σ}_{out}, W	P^{Σ}_{th}, W	η^{Σ}, %	P_{out}, W	P_{th}, W	η, %	$\eta_{q2(max)}$
90% / 4%	Exp.	1.13	0.10	64.2	0.23	0.68	17.8	–
	Calc.	*0.99*	*<0.1*	*37.4*	*0.23*	*<0.2*	*12.0*	***0.91***
97% / 1.3%	Exp.	0.71	0.11	40.9	0.09	0.64	6.8	–
	Calc.	*0.84*	*<0.1*	*37.1*	*0.10*	*<0.2*	*5.1*	***0.93***

*P_{out} –output power, P_{th} – threshold incident power, η – slope efficiency *vs.* the incident pump power (the values with "Σ": emission at both the $^3H_4 \rightarrow {}^3H_5$ and $^3F_4 \rightarrow {}^3H_6$ transitions, without "Σ": emission at the $^3H_4 \rightarrow {}^3H_5$ transition, $\eta_{q2(max)}$ – pump quantum efficiency at the maximum pump power.

The model reasonably explains the observed output power at ~2.3 μm while it predicts lower values for the laser threshold. The maximum η_{q2} values are still below 1 in agreement with the prediction for simultaneous operation at

the $^3H_4 \rightarrow {}^3H_5$ and $^3F_4 \rightarrow {}^3H_6$ transitions, Fig. 12(b).

V. Conclusions

To conclude, the laser operation at the $^3H_4 \rightarrow {}^3H_5$ Tm^{3+} transition is a promising route towards efficient mid-IR bulk and waveguide oscillators operating around ~2.3 μm. Under the condition that the competitive $^3F_4 \rightarrow {}^3H_6$ laser channel is suppressed, a pump quantum efficiency of more than unity (potentially, up to 2) can be achieved thus leading to a laser slope efficiency well exceeding the Stokes limit. This is due to the energy-transfer upconversion acting against cross-relaxation and populating the upper laser level. Strong ETU is linked to the use of moderate and high Tm^{3+} doping levels that simultaneously bring high pump absorption efficiency and, in part, to the adjusted pump mode size.

Fluoride $LiYF_4$ crystals with moderate Tm^{3+} doping levels of few at.% appear as excellent candidates for highly-efficient ~2.3 μm lasers because of a combination of easy Tm^{3+} doping, low phonon energies and good thermo-mechanical properties of the host crystal and suitable spectroscopic behavior of the dopant Tm^{3+} ions. In the present work, we report on a compact bulk 3.5 at.% Tm:$LiYF_4$ laser generating a maximum output power of 0.72 W (quasi-CW operation) at 2306 μm with a record-high slope efficiency of 47.3% versus the absorbed pump power (thus overcoming the Stokes efficiency, 34.4%). We show the first experimental evidence of more than unity pump quantum efficiency in this laser. By applying diode pumping, the power scaling strategy is demonstrated with a clear potential for improvement.

We also report on the first ~2.3 μm Tm waveguide laser based on epitaxially-grown 6.2 at.% Tm:$LiYF_4$ layers. Due to the simultaneous operation of the waveguide laser at both the $^3H_4 \rightarrow {}^3H_5$ and $^3F_4 \rightarrow {}^3H_6$ transitions, the pump quantum efficiency was upper-limited to be less than unity despite the high Tm^{3+} doping level. The laser generated 0.23 W at 2304-2307 nm with a slope efficiency of 19.8% versus the absorbed pump power. Further efforts on ~2.3 μm Tm waveguide lasers should be focused on suppression of laser operation at the high-gain $^3F_4 \rightarrow {}^3H_6$ transition, e.g., by dielectric coatings.

Our conclusions about the mechanism of ~2.3 μm laser operation are valid for other Tm^{3+}-doped fluoride crystals, such as CaF_2, $LiLuF_4$, BaY_2F_8, or even other oxide hosts. A comparative study of CR and ETU parameters of these materials is required to select the best fluoride gain material for the laser operation at the $^3H_4 \rightarrow {}^3H_5$ transition.

References

[1] F. J. McAleavey, J. O'Gorman, J. F. Donegan, B. D. MacCraith, J. Hegarty, and G. Mazé, "Narrow linewidth, tunable Tm^{3+}-doped fluoride fiber laser for optical-based hydrocarbon gas sensing," *IEEE J. Sel. Top. Quantum Electron.*, vol. 3, No. 4, pp. 1103–1111, Aug. 1997.

[2] M. E. Webber, J. Wang, S. T. Sanders, D. S. Baer, and R. K. Hanson, "In situ combustion measurements of CO, CO_2, H_2O and temperature using diode laser absorption sensors," *Proc. Combust. Inst.*, vol. 28, no. 1, pp. 407–413, 2000.

[3] F. J. McAleavey, J. O'Gorman, J. F. Donegan, J. Hegarty, and G. Maze, "Extremely high sensitivity gas detection at 2.3 μm using a grazing incidence Tm^{3+} fibre laser cavity," *Sens. Actuator A – Phys.,* vol. 87, no. 3, pp. 107–112, Jan. 2001.

[4] J. Cihelka, I. Matulková, and S. Civiš, "Laser diode photoacoustic and FTIR laser spectroscopy of formaldehyde in the 2.3 μm and 3.5 μm spectral range," *J. Molec. Spectr.,* vol. 256, no. 1, pp. 68–74, July 2009.

[5] A. Garnache, A. Liu, L. Cerutti, and A. Campargue, "Intracavity laser absorption spectroscopy with a vertical external cavity surface emitting laser at 2.3 μm: Application to water and carbon dioxide," *Chem. Phys. Lett.*, vol. 416, no. 1-3, pp. 22–27, Nov. 2005.

[6] S. T. Fard, W. Hofmann, P. T. Fard, G. Bohm, M. Ortsiefer, E. Kwok, M. C. Amann, and L. Chrostowski, "Optical absorption glucose measurements using 2.3 μm vertical-cavity semiconductor lasers," *IEEE Photon. Technol. Lett.*, vol. 20, no. 11, pp. 930-932, June 2008.

[7] I. T. Sorokina, E. Sorokin, S. Mirov, V. Fedorov, V. Badikov, V. Panyutin, and K. I. Schaffers, "Broadly tunable compact continuous-wave Cr^{2+}:ZnS laser," *Opt. Lett*., vol. 27, no. 12, pp. 1040-1042, June 2002.

[8] G. J. Wagner, T. J. Carrig, R. H. Page, K. I. Schaffers, J.-O. Ndap, X. Ma, and A. Burger, "Continuous-wave broadly tunable Cr^{2+}:ZnSe laser," *Opt. Lett*., vol. 24, no. 1, pp. 19-21, Jan. 1999.

[9] L. Cerutti, A. Garnache, A. Ouvrard, M. Garcia, and F. Genty, "Vertical cavity surface emitting laser sources for gas detection," *Phys. Status Solidi A*, vol. 202, no. 4, pp. 631-635, Feb. 2005.

[10] E. Geerlings, M. Rattunde, J. Schmitz, G. Kaufel, H. Zappe, and J. Wagner, "Widely tunable GaSb-based external cavity diode laser emitting around 2.3 μm," *IEEE Photon. Technol. Lett*, vol. 18, no. 18, pp. 1913-1915, Sept. 2006.

[11] R. Wang, S. Sprengel, A. Malik, A. Vasiliev, G. Boehm, R. Baets, M. C. Amann, and G. Roelkens, "Heterogeneously integrated III–V-on-silicon 2.3μm distributed feedback lasers based on a type-II active region," *Appl. Phys. Lett*, vol. 109, no. 22, pp. 221111, Nov. 2016.

[12] G. Boehm, A. Bachmann, J. Rosskopf, M. Ortsiefer, J. Chen, A. Hangauer, R. Meyer, R. Strzoda, and M.C. Amann, "Comparison of InP- and GaSb-based VCSELs emitting at 2.3 μm suitable for carbon monoxide detection," *J. Cryst. Growth*, vol. 323, no. 1, pp. 442-445, May 2011.

[13] R. C. Stoneman, and L. Esterowitz, "Efficient, broadly tunable, laser-pumped Tm:YAG and Tm:YSGG cw lasers," *Opt. Lett*., vol. 15, no. 9, pp. 486-488, May 1990.

[14] K. van Dalfsen, S. Aravazhi, C. Grivas, S. M. García-Blanco, and M. Pollnau, "Thulium channel waveguide laser with 1.6 W of output power and ~80% slope efficiency," *Opt. Lett*., vol. 39, no. 15, pp. 4380-4383, Aug. 2014.

[15] H. P. Jenssen, A. Linz, R. P. Leavitt, C. A. Morrison, and D. E. Wortman, "Analysis of the optical spectrum of Tm^{3+} in $LiYF_4$," *Phys. Rev. B*, vol. 11, no. 1, pp. 92-101, Jan. 1975.

[16] J. Caird, L. DeShazer, and J. Nella, "Characteristics of room-temperature 2.3-μm laser emission from Tm^{3+} in YAG and $YAlO_3$," *IEEE J. Quantum Electron.*, vol. 11, no. 11, pp. 874-881, Nov. 1975.

[17] J. F. Pinto, L. Esterowitz, and G. H. Rosenblatt , "Tm^{3+}:YLF laser continuously tunable between 2.20 and 2.46 μm," *Opt. Lett.*, vol. 19, no. 12, pp. 883-885, June 1994.

[18] D. Bar-Joseph, "2.32-micron flash-lamp-pumped high-repetition-rate laser operation in Tm:Cr:YAG," *Proc. SPIE,* vol. 1627, pp. 81-85, June 1992.

[19] V. Sudesh, and J.A. Piper, "Spectroscopy, modeling, and laser operation of thulium-doped crystals at 2.3 μm," *IEEE J. Quantum Electron.*, vol. 36, no. 7, pp. 879-884, July 2000.

[20] F. Canbaz, I. Yorulmaz, and A. Sennaroglu, "2.3-μm Tm^{3+}:YLF laser passively Q-switched with a Cr^{2+}:ZnSe saturable absorber," *Opt. Lett.*, vol. 42, no. 9, pp. 1656-1659, May 2017.

[21] A. Braud, S. Girard, J. L. Doualan, M. Thuau, R. Moncorgé, and A. M. Tkachuk, "Energy-transfer processes in Yb:Tm-doped KY_3F_{10}, $LiYF_4$, and BaY_2F_8 single crystals for laser operation at 1.5 and 2.3 μm," *Phys. Rev. B*, vol. 61, no. 8, pp. 5280-5292, Feb.2000.

[22] A. Diening, P.A. Möbert, and G. Huber, "Diode-pumped continuous-wave, quasi-continuous-wave, and Q-switched laser operation of Yb^{3+}, Tm^{3+}:$YLiF_4$ at 1.5 and 2.3 μm," *J. Appl. Phys.*, vo. 84, no. 11, pp. 5900-5904, Nov. 1998.

[23] P. S. F. De Matos, N. U. Wetter, L. Gomes, I. M. Ranieri, and S. L. Baldochi, "A high power 2.3 μm Yb:Tm:YLF laser diode-pumped simultaneously at 685 and 960 nm," *J. Opt. A*, vol.10, no. 10, pp. 104009-1-7, Aug. 2008.

[24] G. J. Kintz, L. Esterowitz, and R. Allen, "Cascade laser emission at 2.31 and 2.08 μm from laser diode pumped Tm,Ho:$LiYF_4$ at room temperature," *in Advanced Solid State Lasers, 26 October 1987,*

Williamsburg, Virginia United States: OSA Technical Digest, 1987, vol. paper MC2.

[25] I. Yorulmaz, and A. Sennaroglu, "Low-threshold diode-pumped 2.3-µm Tm^{3+}: YLF lasers," *IEEE J. Sel. Top. Quantum Electron.*, vol. 24, no. 5, pp. 1601007-1-7, Sept-Oct. 2018.

[26] F. Canbaz, I. Yorulmaz, and A. Sennaroglu, "Kerr-lens mode-locked 2.3-µm Tm^{3+}:YLF laser as a source of femtosecond pulses in the mid-infrared," *Opt. Lett.*, vol. 42, no.19, pp. 3964-3967, Oct. 2017.

[27] R. Soulard, A. Tyazhev, J.L. Doualan, A. Braud, A. Hideur, M. Laroche, B. Xu, and P. Camy, "2.3 µm Tm^{3+}:YLF mode-locked laser," *Opt. Lett.*, vol. 42, no. 18, pp. 3534-3536, Sept. 2017.

[28] R. Allen, and L. Esterowitz, "CW diode pumped 2.3 µm fiber laser," *Appl. Phys. Lett.*, vol. 55, no. 8, pp. 721-722, June 1989.

[29] J. N. Carter, D. C. Hanna, R. G. Smart, and A. C. Tropper, "Thulium-doped fluorozirconate fiber lasers operating at around 0.8, 1.47, 1.9, and 2.3 µm pumped at 0.79 µm," *in Advanced Solid State Lasers, 18 March 1991, Hilton Head, South Carolina, United States*: OSA Proceedings Series, 1991, vol. 10, paper. MIL13.

[30] R.M. El-Agmy, and N.M. Al-Hosiny, "2.31 µm laser under up-conversion pumping at 1.064 µm in Tm^{3+}: ZBLAN fibre lasers," *Electron. Lett.*, vol. 46, no. 13, pp. 936-937, June 2010.

[31] S. V. Muravyev, E. A. Anashkina, A. V. Andrianov, V. V. Dorofeev, S. E. Motorin, M. Y. Koptev, and A. V. Kim, "Dual-band Tm^{3+}-doped tellurite fiber amplifier and laser at 1.9 µm and 2.3 µm," *Sci. Rep.*, vol. 8, no. 1, pp. 16164, Nov. 2018.

[32] C. Jia, B.J. Shastri, P.R. Prucnal, M. Saad, and L. R. Chen, "Simultaneous Q-switching of a Tm^{3+}:ZBLAN fiber laser at 1.9 µm and 2.3 µm using graphene," *IEEE Photon. Technol. Lett.*, vol. 29, no. 4, pp. 405-408, Jan. 2017.

[33] M. Schellhorn, "High-power diode-pumped Tm:YLF laser," *Appl. Phys. B*, vol. 91, no. 1, pp. 71–74, Apr. 2008.

[34] P. Loiko, J. M. Serres, X. Mateos, S. Tacchini, M. Tonelli, S. Veronesi, D. Parisi, A. Di Lieto, K. Yumashev, U. Griebner, and V. Petrov, "Comparative spectroscopic and thermo-optic study of Tm:LiLnF$_4$ (Ln = Y, Gd, and Lu) crystals for highly-efficient microchip lasers at ~2 µm," *Opt. Mater. Express*, vol. 7, no. 3, pp. 844-854, Mar. 2017.

[35] S. A. Miller, H. E. Rast, and H. H. Caspers, "Lattice vibrations of LiYF4," *J. Chem. Phys*., vol. 52, no. 8, pp. 4172-4175, Apr. 1970.

[36] R. L. Aggarwal, D. J. Ripin, J. R. Ochoa, and T. Y. Fan, "Measurement of thermo-optic properties of $Y_3Al_5O_{12}$, $Lu_3Al_5O_{12}$, $YAlO_3$, $LiYF_4$, $LiLuF_4$, BaY_2F_8, $KGd(WO_4)_2$, and $KY(WO_4)_2$ laser crystals in the 80–300 K temperature range," *J. Appl. Phys.*, vol. 98, no. 10, pp. 103514-1-14, Nov. 2005.

[37] B. Cockayne, J. G. Plant, and R. A. Clay, "The Czochralski growth and laser characteristics of Li(Y,Er,Tm,Ho)F_4 and Li(Lu,Er,Tm,Ho)F_4 scheelite single crystals," J. Cryst. Growth, Vol. 54, No. 3, pp.407-413, Sept. 1981.

[38] B. M. Walsh, N. P. Barnes, and B. Di Bartolo, "Branching ratios, cross sections, and radiative lifetimes of rare earth ions in solids: Application to Tm^{3+} and Ho^{3+} ions in $LiYF_4$," *J. Appl. Phys.*, vol. 3, no. 5, pp. 2772-2787, Mar. 1998.

[39] S. So, J. I. Mackenzie, D. P. Sheperd, W. A. Clarkson, J. G. Betterton, and E. K. Gorton, "A power-scaling strategy for longitudinally diode-pumped Tm:YLF lasers," *Appl. Phys. B*, vol. 84, no. 3, pp. 389–393, Sept. 2006.

[40] B. Aull, and H. Jenssen, "Vibronic interactions in Nd:YAG resulting in nonreciprocity of absorption and stimulated emission cross sections," *IEEE J. Quantum Electron*., vol. 18, no. 5, pp. 925-930, May 1982.

[41] N. P. Barnes and D. J. Gettemy, "Temperature variation of the refractive indices of yttrium lithium fluoride," *J. Opt. Soc. Am*., vol. 70, no. 10, pp. 1244-1247, Oct. 1980.

[42] C. Görller-Walrand, and K. Binnemans, "Spectral intensities of f-f transitions," Handbook on the physics and chemistry of rare earths, vol. 25, pp.101-264, 1998.

[43] I. Razumova, A. Tkachuk, A. Nikitichev, and D. Mironov, "Spectral-luminescent properties of Tm:YLF crystal," J. Alloy Compd., vol. 225, no. 1-2, pp. 129-132, July 1995.

[44] G. Armagan, A. M. Buoncristiani, A. T. Inge, and B. Di Bartolo, "Comparison of spectroscopic properties of Tm and Ho in YAG and YLF crystals," *in Advanced Solid State Lasers, 18 March 1991, Hilton Head, South Carolina, United States*: OSA Proceedings Series, 1991, vol. 10, paper. MIL14.

[45] A. M. Tkachuk, I. K. Razumova, E. Y. Perlin, M. F. Joubert, and R. Moncorge, "Luminescence self-quenching in Tm^{3+}:YLF crystals: II. The luminescence decay and macrorates of energy transfer," *Opt. Spectr*., vol. 90, no. 1, pp. 78-88, Jan. 2001.

[46] A. Braud, "Caractéristiques spectroscopiques et émission laser de l'ion Tm^{3+} à 1.5 µm dans les fluorures," PhD thesis, Caen University, 1999 [In French].

[47] R. Soulard, M. Salhi, G. Brasse, P. Loiko, J.L. Doualan, L. Guillemot, A. Braud, A. Tyazhev, A. Hideur, and P. Camy, "Laser operation of highly-doped Tm:$LiYF_4$ epitaxies: Towards thin-disk lasers," *Opt. Express*, vol. 27, no. 6, pp. 9287-9301, Mar. 2019.

[48] B. M. Walsh, N. P. Barnes, M. Petros, J. Yu, and U. N. Singh, "Spectroscopy and modeling of solid state lanthanide lasers: Application to trivalent Tm^{3+} and Ho^{3+} in $YLiF_4$ and $LuLiF_4$," *J. Appl. Phys*., vol. 95, no. 7, pp. 3255-3271, Apr. 2004.

[49] P. Loiko, and M. Pollnau, "Stochastic model of energy-transfer processes among rare-earth ions. Example of Al_2O_3:Tm^{3+}," *J. Phys. Chem. C*, vol. 120, no. 46, pp. 26480-26489, Nov. 2016.

[50] E. C. Honea, R. J. Beach, S. B. Sutton, J. A. Speth, S. C. Mitchell, J. A. Skidmore, M. A. Emanuel, and S. A. Payne, "115-W Tm:YAG diode-pumped solid-state laser," *IEEE J. Quantum Electron*., vol. 33, no. 9, pp. 1592-1600, Sept. 1997.

[51] P. Loiko, P. Koopmann, X. Mateos, J. M. Serres, V. Jambunathan, A. Lucianetti, T. Mocek, M. Aguiló, F. Díaz, U. Griebner, V. Petrov, and C. Kränkel, "Highly-efficient, compact Tm^{3+}:RE_2O_3 (RE = Y, Lu, Sc) sesquioxide lasers based on thermal guiding," *IEEE J. Sel. Top. Quantum Electron.*, vol. 24, no. 5, pp. 1600713-1-13, Sept-Oct. 2018.

[52] X. Mateos, P. Loiko, J.M. Serres, K. Yumashev, U. Griebner, V. Petrov, M. Aguiló, and F. Díaz, "Efficient micro-lasers based on highly-doped monoclinic double tungstates," *IEEE J. Quantum Electron*., vol. 53, no. 3, pp. 1700110, June 2017.

[53] M. Falconieri, A. Lanzi, G. Salvetti, and A. Toncelli, "Fluorescence dynamics in Tm,Ho:YLF following 800 nm pulsed laser excitation," *Appl. Phys. B*, vol. 66, no. 2, pp. 153-162, Feb. 1998.

[54] P. Loiko, R. Soulard, G. Brasse, J.L. Doualan, B. Guichardaz, A. Braud, A. Tyazhev, A. Hideur, and P. Camy. "Watt-level Tm:$LiYF_4$ channel waveguide laser produced by diamond saw dicing," *Opt. Express*, vol. 26, no.19, pp. 24653-24662, Sept. 2018.

[55] E. Y. Perlin, A. M. Tkachuk, M. F. Joubert, and R. Moncorge, "Cascade-avalanche up-conversion in Tm^{3+}:YLF crystals," *Opt. Spectr*., vol. 90, no. 5, pp. 691-700, May 2001.

[56] D. Findlay, and R. A. Clay, "The measurement of internal losses in 4-level lasers," *Phys. Lett*., vol. 20, no. 3, pp. 277-278, Feb. 1966.